Desalination and Water Treatment
www.deswater.com
doi: 10.5004/dwt.2020.25940

197 (2020) 237–248
September

Corrosion mechanisms of ductile iron pipes in water distribution system: impacts of ionic strength and cement mortar lining coverage

Haiya Zhang, Dibo Liu, Lvtong Zhao, Xiaojian Zhang, Jun Wang, Chao Chen*

School of Environment, Tsinghua University, Beijing 100084, China, emails: chen_water@mail.tsinghua.edu.cn (C. Chen), flying850612@126.com (H. Zhang), liudb16@mails.tsinghua.edu.cn (D. Liu), zhaolvtong@qq.com (L. Zhao), zhangxj@mail.tsinghua.edu.cn (X. Zhang), wangjun2008@tsinghua.edu.cn (J. Wang)

Received 28 November 2019; Accepted 4 April 2020

ABSTRACT

The corrosion process of the ductile iron pipes with different cement mortar lining coverage (lined (100%), unlined (0%), 50%, and 90% lining coverage) in water containing chloride and sulfate were investigated. Electrochemical measurements, including the potentiodynamic polarization curves and electrochemical impedance spectra methods, were carried out to analyze the corrosion mechanisms. Results indicated that the maximum corrosion potential of ductile iron pipes decreased as the increment of ionic strength in a logarithm tendency, while the corrosion current density increased linearly with ionic strength. Additionally, the cement mortar lining coverage affects the inner ductile iron corrosion significantly. The corrosion rate of unlined ductile iron was about 2–5 times higher than that of lined ductile iron pipes. Different from the corrosion rate of lined ductile iron pipes, that of ductile iron pipes with minor defects (90% lining) was higher in the first 10 d, followed by a lower one. The cement mortar lining coverage with significant defects (50% of lining) showed poor protection ability on the iron surface. Moreover, a roughly linear correlation between average corrosion rate (mm a^{-1}) and the relative proportion of bare ductile iron area was fitted.

Keywords: Corrosion damage mechanisms; Chloride; Sulfate; Ductile iron pipes; Cement mortar lining; Water distribution system

1. Introduction

Ductile iron pipes lined with cement mortar are the ideal pipes for tap water transportation according to the research of the American Water Engineering Association [1]. These pipes have been widely used in water distribution systems worldwide because of their high strength, large diameter, and excellent durability, which was reported accounted for more than 80% of the total water supply pipe materials for water mains in China [2]. However, in many investigations of the actual operating water distribution system, the cement mortar lining degradation caused by erosion of transporting water, damage of external forces often occurred frequently [3,4]. This degradation could induce the internal metal pipe corrosion, pipes service life reduction, and water quality deterioration in water distribution systems [5]. Therefore, tracking the complex corrosion process of ductile iron pipes involving the cement mortar lining degradation was necessary and might be important for the water supply safety of the water companies worldwide.

The aggressive anions, especially the chloride and sulfate ions were reported as the primary cause of cement mortar film breakdown [6]. These ions could penetrate through the cement mortar/metal surface and change the inner metal corrosion mechanisms [7]. However, as far as we know, the related research was mainly focused on the steel bars embedded in the concrete. The corrosion damage mechanisms of steel bars induced by the chlorides have been extensively studied in the last few years, mainly involving the critical chloride content (C_{crit}) or chloride threshold value

* Corresponding author.

(Cl_{th}) in the concrete pore solution [8,9]. C_{crit} and Cl_{th} were considered the threshold for initiating the de-passivation or corrosion of the reinforcement. Research also showed that the open circuit potential (OCP) of reinforcement decreased and corrosion current density (i_{corr}) increased with the increase of the $[Cl^-]/[OH^-]$ ratio in simulated concrete pore solution [8]. Additionally, some research also depicted the relationship between different electrochemical parameters (OCP, polarization resistance (R_p) and i_{corr}) as a function of $[Cl^-]/[OH^-]$ for the concrete pore solution [10].

Sulfate (SO_4^{2-}) was another critical factor concerning the corrosion behavior of reinforcing steel in concrete. The sulfate ions could accelerate the active dissolution of iron by forming soluble complexes with either Fe^{2+} or Fe^{3+} and cause uniform corrosion [11,12]. The high SO_4^{2-} concentration (0.05 mol L^{-1}) could induce the decrement of corrosion potential and acceleration of corrosion process for reinforcing steel [13]. Additionally, sulfate ions could attack various hydration products of cement, resulting in the formation of different compounds [14]. In a typical tap water distribution system, both chloride and sulfate ions are present. When iron pipes are subjected to both chloride-induced reinforcement corrosion and sulfate attack, the deterioration mechanism may become even more complicated because of the ingress these two types of ions [15]. Some different phenomena were observed when the two ions coexist. The sulfate ions could decrease the corrosion rate of the steel in chloride-induced corrosion process [12]. Furthermore, sulfate ions may mitigate the chance of pitting corrosion of steel reinforcement caused by chloride in the concrete mixes containing both ions [16].

Electrochemical tests provided us with valuable information for the corrosion initiation and passivity, but they could not create a complicated condition that present in the concrete/metal interface, such as the inhomogeneity, oxygen diffusion, etc. Research found that the corrosion reaction occurred predominantly at the breaks or at the imperfections of the partially protective film [17]. Horne et al. [18] confirmed that the gaps between the steel surface and concrete experienced more corrosion than the other areas. Ming et al. [19] research indicated that the Cl_{th} values were significantly lower in defective areas on the steel surface than that with a passive layer formation on the surface. Alonso et al. [20] reported a higher susceptibility to corrosion for ribbed steel bars in comparison to that of smoothed bars. Hence, understanding the corrosion behaviors under different lining/metal interface is of great importance for engineering applications [21]. However, most of the research focuses on the steels embedded in the concrete, but not the corrosion behavior of ductile iron with different defective cement mortar lining interface.

Thus, ductile iron pipes with different cement mortar lining coverage were designed and produced to carry out the corrosion damage experiments in water with low, intermediate, and high concentrations of anions. Electrochemical measurements, such as polarization curves and electrochemical impedance spectra (EIS), were conducted to analyze the corrosion process. The objectives of this study include (1) to analyze the effect of ionic strength on the corrosion potential and corrosion current density, (2) to investigate the effect of different cement lining coverage on the corrosion process of inner ductile iron pipes, (3) to illustrate the electrochemical corrosion mechanism for ductile iron pipes with different cement mortar lining coverage in water with a high concentration of anions.

2. Materials and methods

2.1. Ductile iron electrodes preparation

The chemical composition of the ductile iron pipes are as follows: C 19.08%, Si 2.06%, O 6.09%, P 0.65%, Ca 0.58%, S 1.60%, Cu 1.98%, Mn 0.92%, Zn 2.04%, and Fe for balances. The iron coupon was cut into a cylinder with an exposed area of 0.5 cm^2, and then this cylinder was mounted with epoxy resin and connected with the testing equipment through the copper wires. The ductile iron surface was washed with acetone and absolute ethyl alcohol, and then were prepared for the cement mortar injecting. The cement used in the presented study was the Portland cement (42.5) with the chemical composition shown in Table 1.

The cement mortar was firstly prepared according to the mixture proportion (mass ration of water, cement, and sand is 1:0.5:1.5), and was then injected into the ductile iron electrodes to a thickness of 10 mm, according to the coating standard [4]. Afterwards, the prepared samples were put into the drying room for natural curing for 24 h and into the humidity chamber (humidity 99% RH, temperature 20°C ± 2°C) for steam curing for 7 d consecutively. The area of working electrode was 0.5 cm^2, with an inner diameter of 7 cm and an outer diameter of 10 cm, a 10 mm-thick cement mortar lining layer and a 10 mm-thick ductile iron layer. Fig. 1 shows the section and layout diagrams of the ductile iron with different cement mortar lining coverage after curing (a) lined ductile iron (100% lining), (b) ductile iron with 90% lining, (c) ductile iron with 50% lining, and (d) unlined ductile iron (0%).

2.2. Solution preparation and experimental design

The corrosion process of ductile iron pipes with different lining coverage in deionized water was used as a reference. The water quality of deionized water was as follows: dissolved oxygen (DO): 7.04 mg L^{-1}, pH: 5.4, conductivity: 3.55 μs cm^{-1}, oxidation–reduction potential (ORP): 258.8 mV, alkalinity-$CaCO_3$: 0.0 mg L^{-1}, hardness: 0.0 mg L^{-1}. Then sodium chloride reagent with a density of 3.297 g L^{-1} at room temperature was used to prepare a

Table 1
Composition of the ordinary Portland cement (%)

Composition	Content
SiO_2	20.6
Al_2O_3	5.01
SO_3	2.68
CaO	63.9
Fe_2O_3	3.25
K_2O	0.65
Na_2O	0.3

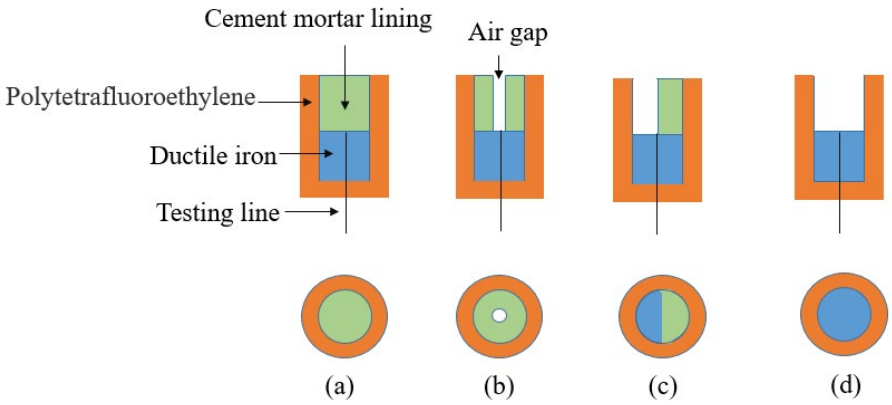

Fig. 1. Section and layout diagram of ductile iron with different proportions of lining.

specific concentration of chloride solution with deionized water (Tianjin Guangfu Technology Development Co., Ltd., Tianjin, China). Similarly, sodium sulfate regent with a density of 2.957 g L^{-1} was used to prepare the sulfate solution with deionized water (Tianjin Guangfu Technology Development Co., Ltd., Tianjin, China). The prepared ductile iron electrodes with different cement mortar lining coverage were immersed into the low (40 mg L^{-1} Cl^- + 80 mg L^{-1} SO_4^{2-}), intermediate (120 mg L^{-1} Cl^- + 80 mg L^{-1} SO_4^{2-}) and high (120 mg L^{-1} Cl^- + 240 mg L^{-1} SO_4^{2-}) concentration solution respectively for a 50 d experiment. The experimental design and the serial number of immersion tests are shown in Table 2. The contrastive analysis of (1, 2, 3), (4, 5, 6), (7, 8, 9), and (10, 11,12) can give an analysis of ionic strength on the corrosion process of ductile iron with different lining coverage; the comparison of serial numbers (1, 4, 7, 10), (2, 5, 8, 11), and (3, 6, 9, 12) can give a full analysis of the effect of lined surface coverage on the inner ductile iron corrosion process.

2.3. Electrochemical measurements

The corrosion damage mechanisms of ionic strength on the ductile iron with different lining coverage were analyzed by electrochemical methods, in a three-electrode configuration. In addition to the prepared working electrode, an Ag/AgCl (saturated KCl) functioned as the reference electrode, and a high purity platinum sheet (1.0 cm^2) was used as the counter electrode. All the electrochemical measurements were carried out using an electrochemical working station (Wuhan Corrtest Instruments Corp., Ltd., Wuhan City, China) equipped with 16 channel expanders. The electrochemical test and signal collecting system are shown in Fig. 2.

The corrosion potential (E_{corr}) was measured after the system was stable. The non-destructive linear polarization resistance was used to calculate the corrosion current density (I_{corr}) and corrosion rate (mm a^{-1}). The applied voltage of the polarization sweep was ±100 mV to E_{corr}, and the scan rate was 10 mV s^{-1}. EIS was employed to acquire the lining coverage information on the ductile iron surface. The impedance system had an amplitude of 10 mV and a frequency of 10^{-2} to 10^5 Hz, in which 10 points were measured at each stage. The obtained Nyquist and Bode plots were simulated by the corresponding equivalent electrical circuit through the ZsimpView software.

2.4. Corrosion scales collection

After 50 d exposure, the working electrodes were extracted, which were inspected by JSM-7001F field emission scanning electron microscopy (SEM) (JEOL, Tokyo City, Japan) for the corrosion morphology and by the energy dispersive spectrometer (EDS) for the elemental composition analysis. Before observation, the specimens were also placed in a freeze dryer (FDU-1100) (Tokyo Rikakikai Co., Ltd., Tokyo City, Japan) for 24 h to dehydrate.

3. Results and discussion

3.1. Impact of cement mortar lining coverage on corrosion potential

The corrosion potential (E_{corr}) is an important factor to reflect the surface corrosion tendency [22,23]. Fig. 3 depicts the time-dependent E_{corr} values of ductile iron pipes with different proportion of cement mortar lining in water with 40 mg L^{-1} Cl^- and 80 mg L^{-1} SO_4^{2-}.

The E_{corr} of unlined ductile iron exposed to this solution was more negative (–0.678 to –0.725 V) throughout the whole experiments, suggesting the severe corrosion risk according to research results of Song (<–0.406 V) [24]). This process might be caused by the strong attack of chloride and sulfate ions on the bare ductile iron surface. However, compared with that of unlined ductile iron, E_{corr} of ductile iron with other proportion of cement mortar lining shifted in a more noble direction, indicating the obvious protection effect of lining itself.

The E_{corr} of ductile iron with 50% cement mortar lining showed a slightly increasing trend with the exposure time, but all values were always in the region of severe corrosion risk (<–0.406 V). While, the different phenomenon can be seen in the case of ductile iron with 90% lining: the potential moved basically in a positive direction during the exposure time, with E_{corr} parameters transforming from –0.526 to –0.187 V, experiencing the stages of severe corrosion risk

Table 2
Experimental design and the serial number of immersion test

Category	Chloride, sulfate ions concentration (mg L^{-1})		
	40, 80	120, 80	120, 240
Lined ductile iron	1	2	3
Ductile iron with 90% lining coverage	4	5	6
Ductile iron with 50% lining coverage	7	8	9
Unlined ductile iron	10	11	12

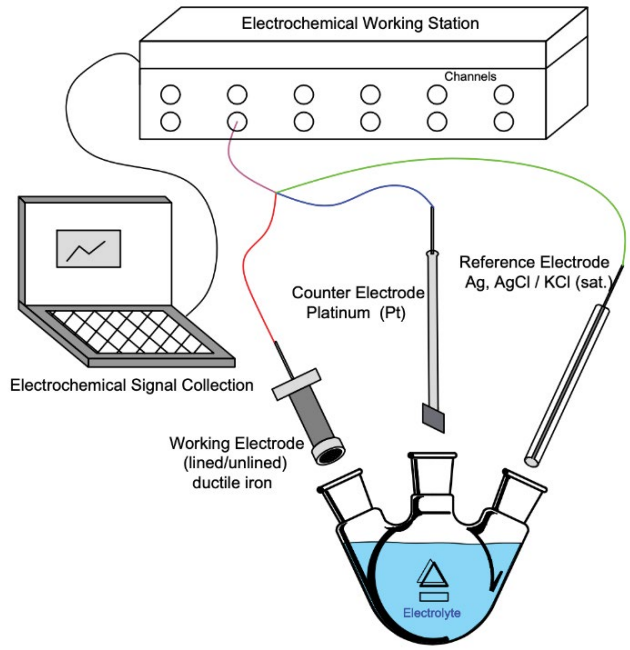

Fig. 2. Electrochemical test and signal collecting system.

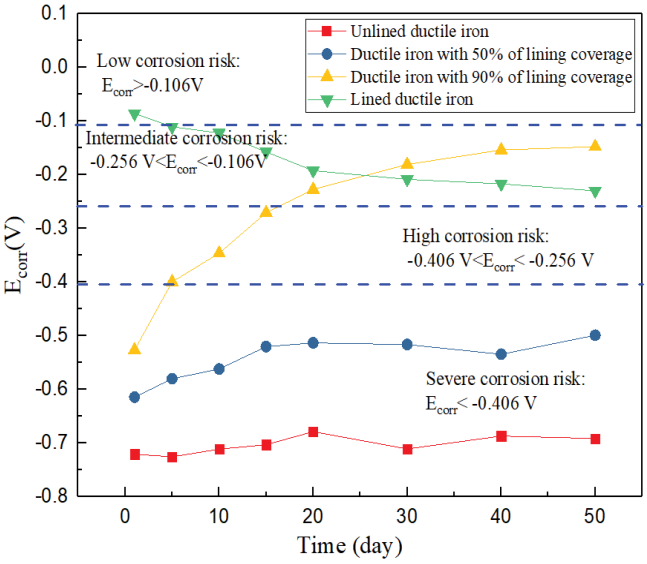

Fig. 3. Corrosion potential evolution of ductile iron pipes with different proportion of cement mortar lining in water with 40 mg L^{-1} Cl^- and 80 mg L^{-1} SO_4^{2-} as exposure of time.

stage (<–0.406 V), high corrosion risk stage (<–0.256 V), and intermediate corrosion risk stage (–0.256 to –0.106 V), revealing the great evolution on the iron surface. This process is most likely related to the hydrolytic and corrosion reaction on the lining/iron interface. The E_{corr} of lined ductile iron were in the low corrosion risk region (>–0.106 V) initially. Subsequently, they decreased gradually and reached the intermediate corrosion region (–0.106 to –0.256 V), suggesting the broken effect of chloride and sulfate anions on the cement mortar lining.

3.2. Impact of ionic strength on corrosion potential

Fig. 4 illustrates the maximum corrosion potential ($E_{corr\text{-}max}$) of ductile iron with different lining coverage under low (40 mg L^{-1} Cl^- + 80 mg L^{-1} SO_4^{2-}), intermediate (120 mg L^{-1} Cl^- + 80 mg L^{-1} SO_4^{2-}), and high (120 mg L^{-1} Cl^- + 240 mg L^{-1} SO_4^{2-}) ionic strength.

$E_{corr\text{-}max}$ is one of the most generally used corrosion indices to evaluate the corrosion reaction on the metal surface. The maximum corrosion potential decreased as the increment of ionic strength, revealing that anions in water promoted the corrosion tendency of iron. $E_{corr\text{-}max}$ of ductile iron with different lining in high ionic strength (120 mg L^{-1} Cl^- + 240 mg L^{-1} SO_4^{2-}) was basically lower than that in intermediate (120 mg L^{-1} Cl^- + 80 mg L^{-1} SO_4^{2-}) experiment, illustrating that the increase of sulfate concentration also caused the decrease of corrosion potential.

The relationship between the $E_{corr\text{-}max}$ and the molar concentration of anions was determined according to the following relation as Eq. (1) [25,26] and the fitting parameters can be seen in Table 3. A logarithmic relationship between the maximum corrosion potential and the concentration of anions was obvious for the unlined, 50% lining and lined ductile iron (0.999, 0.910, and 0.979), which was consistent with the current understanding on the relationship between the corrosion potential and anions concentration for the bare metals [27]. However, this correlation was relatively weaker in the ductile iron with 90% lining (0.673), which might be related to the hydrolytic and corrosion reaction on the heterogeneous lining/iron interface.

$$E_{corr\text{-}max}(V) = A \ln c\left(Cl^- + SO_4^{2-}\right) + B \quad (1)$$

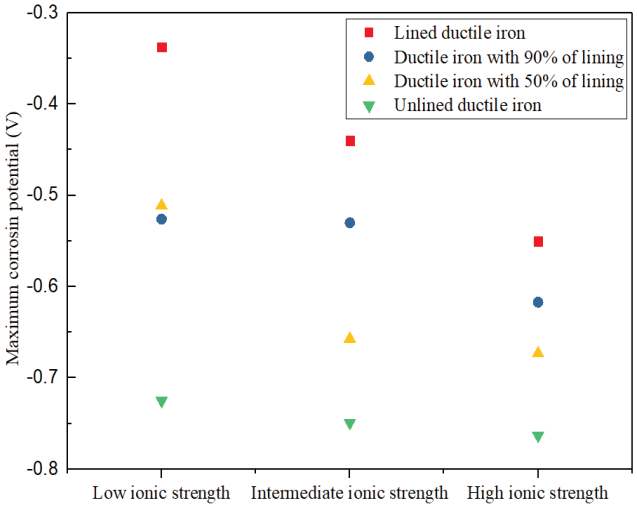

Fig. 4. Maximum corrosion potential of ductile iron with different lining coverage under low, intermediate, and high ionic strength.

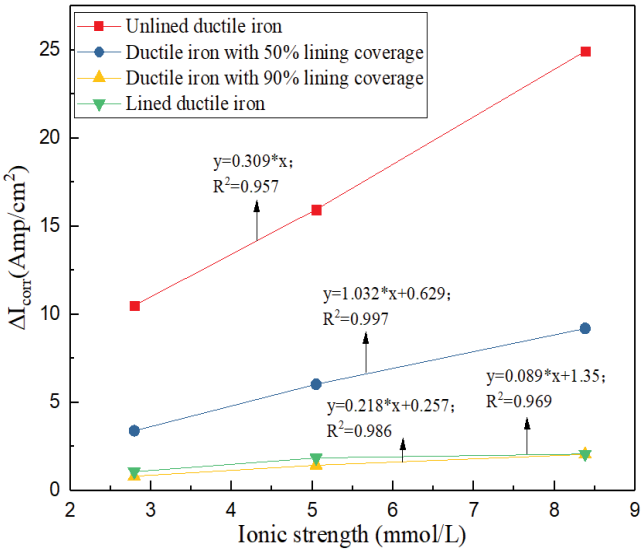

Fig. 5. Relationship between ΔI_{corr} and ionic strength (mmol L^{-1}) for ductile iron electrodes with different lining coverage.

3.3. Impacts of ionic strength on corrosion current density

The corrosion process of ductile iron with different lining coverage in deionized water was used as a reference. The I_{corr} were obtained from the fitted results of the polarization curves. The ΔI_{corr} was defined as the variation of I_{corr} in different ionic strength experiments compared with that in reference experiments (deionized water). Fig. 5 shows the fitted results for the relationship between ΔI_{corr} and ionic strength (mmol L^{-1}) for a ductile iron electrode with different lining coverage.

The values of ΔI_{corr} were all directly proportional to the ionic strength in the solutions and the linear correlation coefficients (R^2) were all higher than 0.950, showing the corrosion promoting effect of chloride and sulfate ions on the ductile iron corrosion process. This phenomenon can be explained by the strong, aggressive performance of chloride and sulfate anions on the iron surface [28].

Additionally, both the slope of fitted lines and the values of ΔI_{corr} increased as the decrease of lining coverage on the ductile iron electrode surface, indicating the blocking effect of cement mortar lining for the anions penetrating on the iron surface. Moreover, no noticeable difference for ΔI_{corr} values was spotted for ductile iron electrodes with 90% and 100% cement mortar lining coverage, verifying that the small defects of cement mortar lining might not affect the corrosion process significantly.

3.4. Ductile iron surface morphology

The surface morphology of ductile iron with different cement mortar lining coverage is shown in Fig. 6. The element composition for the selected area of the SEM can be seen in Table 4.

Some holes and pockmarks were observed on the surface of lined ductile iron after 50 d exposure. From SEM results, some products with needle-like structure and hexagonal-shape plates structure were found. According to the previous research [29], the products were deemed as calcium carbonate and calcium hydroxide respectively. The EDS results also confirmed the presence of large amounts of calcium on the surface. It was speculated that the chloride and sulfate anions might react with the hydrolysis products of cement mortar lining and form $CaCl_2$ or $CaSO_4$, thus causing the damage of cement mortar lining. This reaction could change the smooth cement lining surface into a rough one with holes and pockmarks. Additionally, the internal structure of cement mortar lining became loose and reduced the corrosion resistance. In serious cases, the protection effect of cement mortar lining might fail.

In addition to the calcium oxides, some corrosion products were found for ductile iron with 90% lining. The EDS results also revealed the deposition of iron corrosion products, which were found well-incorporated with calcium carbonate fiber crystal from SEM. The presence of

Table 3
Fitting parameters of maximum E_{corr} and molar concentration of chloride and sulfate ions

Parameters	Unlined ductile iron	50% of lining	90% of lining	Lined ductile iron
A	–0.035	–0.153	–0.076	–0.190
B	–0.695	–0.392	–0.4472	–0.167
R^2	0.999	0.910	0.673	0.979

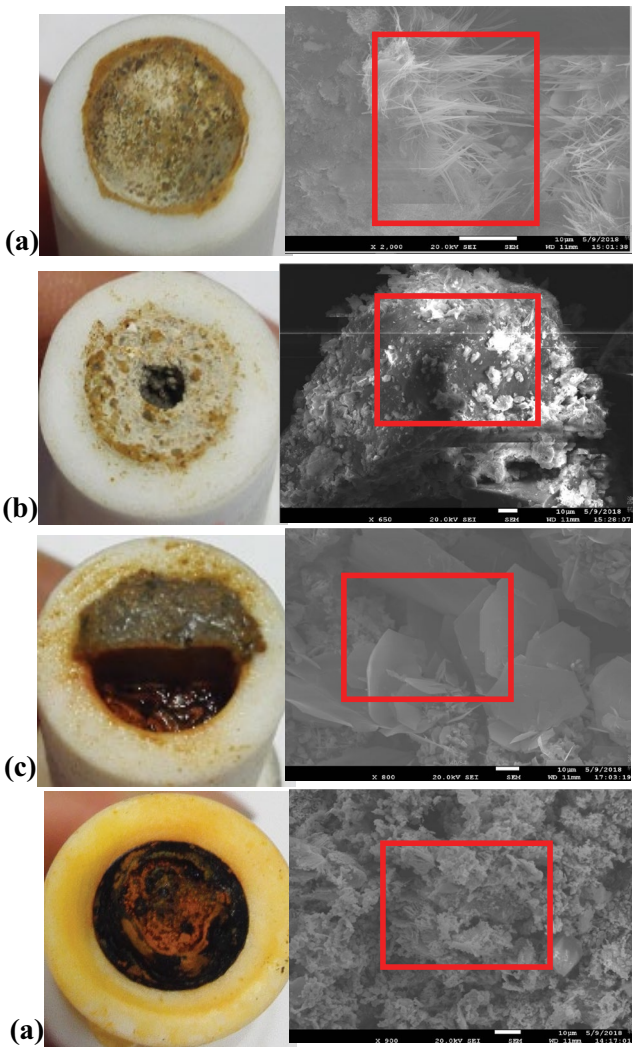

Fig. 6. Morphology of ductile iron pipes with different cement mortar lining coverage (a) lined ductile iron, (b) ductile iron with 90% lining, (c) ductile iron with 50% lining, and (d) unlined ductile iron.

this well-incorporated iron oxides and calcium hydrolysate might protect the iron surface. Previous research also reported that the products composed of iron oxides, iron hydroxides, and calcium oxides on the metal surface could act as a passivation layer [10].

Examination of the ductile iron surface with 50% lining coverage showed that the porous corrosion rust layer with some flake-like lepidocrocite (γ-FeOOH). The unlined ductile iron surface can be seen in Fig. 6d, in which the loose corrosion products with a morphology and chemical composition were different from the case with lined ductile iron pipes. The high content of Fe in this sample also suggested the accumulation of corrosion products.

3.5. Electrochemical impedance spectra analysis

3.5.1. Lined ductile iron pipes

Fig. 7 shows the Nyquist plots of lined ductile iron electrodes in water with high ionic strength (120 mg L^{-1} Cl^- + 240 mg L^{-1} SO_4^{2-}). The electrical circuit model (ECM) in Fig. 7 was used to stimulate the Nyquist plots, in which, R_s is the solution resistance, R_f is the film resistance, R_{ct} is the iron/solution charge transfer resistance, Q_f is the film capacitance, and Q_{ct} is the double-layer capacitance. Additionally, considering the dispersion effect of the double layer at the iron/solution interface, n is a fit parameter ranging from 0 to 1. When n is at 0 and 1, the iron electrode act respectively as a pure resistor and a pure capacitance. The fitted results can be seen in Table 5.

The Nyquist plots in low frequency at 5 d presented a Warburg diffusion phenomenon, showing the good protection ability of cement mortar lining. Therefore, these plots were fitted with the ECM containing Warburg diffusion resistance. After 5 d, the curves in the high-frequency region and low-frequency region all presented a capacitive behavior with the plots decreasing gradually, revealing the damaging effect of chloride and sulfate on the lining.

It was speculated that the chloride and sulfate anions might react with the hydrolysis products of cement mortar lining and form $CaCl_2$ or $CaSO_4$, thus causing the damage of

Table 4
Element composition of ductile iron electrodes with different cement mortar lining coverage

Element (Wt.%)	Lined ductile iron pipe	Ductile iron with 90% of lining coverage	Ductile iron with 50% of lining coverage	Unlined ductile iron pipes
C	0.00	22.71	25.86	21.42
O	0.00	50.29	52.27	10.60
Si	0.00	22.50	0.77	0.59
S	0.96	0.22	0.27	0.10
Cl	0.03	0.00	0.10	0.02
Ca	94.46	3.31	17.99	0.00
Fe	0.00	0.29	1.43	67.27
Zr	0.00	0.00	1.31	0.00
Al	4.55	0.68	0.00	0.00
Mg	0.00	0.00	0.00	0.00
Total	100	100	100	100

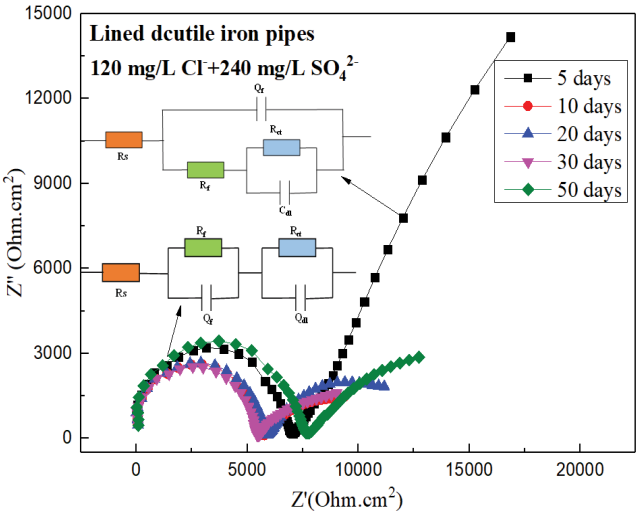

Fig. 7. Nyquist plots of lined ductile iron pipes in water with high ionic strength (120 mg L^{-1} Cl^- + 240 mg L^{-1} SO_4^{2-}).

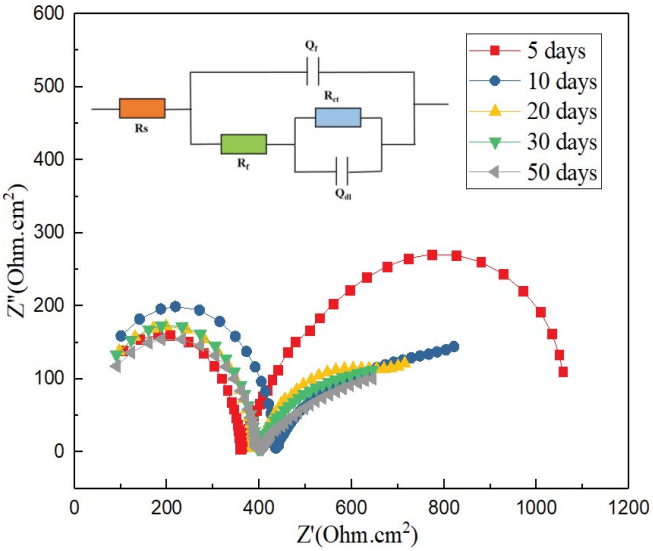

Fig. 8. Nyquist plots of unlined ductile iron pipes in water with high ionic strength.

cement mortar lining. This reaction also promoted the dissolution of calcium hydroxide, increased the lining porosity, and reduced the lining resistance [30]. This would be consistent with the de-passivation theory of film formed on the cement mortar lining/ductile iron interface when the chloride concentration was higher than 10.5 mg L^{-1} [31]. Gerengi et al. [32] also proved the decrement of concrete electrical resistance after 60 d exposure to sulfate attack solution.

Moreover, the fitted Q_{dl} were all between 100 and 1,000 μF cm^{-2}, the range for the corrosion initiation stage [33]. Thus, the obtained electrochemical results confirmed that the durability of cement mortar lining cannot sustain in water with high chloride and sulfate ions strength.

3.5.2. Unlined ductile iron pipes

The Nyquist plots of unlined ductile iron pipes in water with high ionic strength (120 mg L^{-1} Cl^- + 240 mg L^{-1} SO_4^{2-}) are shown in Fig. 8.

The ECM containing two-time constants in Fig. 8 was used to simulate the Nyquist plots. The fitted results are shown in Table 6.

The resistance of R_f maintained relatively lower values and varied slightly between 337.0 to 411.37 Ω cm^2, suggesting the low resistance of the corrosion scale. Meanwhile, the R_{ct} decreased from 821.9 Ω cm^2 at 5 d to 429.4 Ω cm^2 at 50 d. This R_{ct} was lower than that reported for the severe corrosion (14,000 Ω cm^2) [31], showing the rapid corrosion reaction on the iron surface. This reaction might be attributed to the direct attack of chloride and sulfate anions on the iron surface by forming potentially active dissolution sites. In this process, a proportion of ferrous ion at the anode might react with H_2O and form $FeOH^+$ [Eqs. (2)–(4)] and another proportion would be incorporated with the Cl^- and SO_4^{2-} to form ferrous salts in solution [Eqs. (5) and (6)].

$$O_2 + 2H_2O + 4e^- \rightarrow 4OH^- \quad (2)$$

$$Fe \rightarrow Fe^{2+} + 2e^- \quad (3)$$

$$Fe^{2+} + H_2O \rightarrow FeOH^+ + H^+ \quad (4)$$

$$Fe^{2+} + 2Cl^- + 4H_2O \rightarrow FeCl_2 \cdot 4H_2O \quad (5)$$

$$Fe^{2+} + SO_4^{2-} \rightarrow FeSO_4 \quad (6)$$

The formed $FeOH^+$ could be oxidized rapidly and formed γ-FeOOH. γ-FeOOH often appeared as the corrosion products in early stage, which have anions selectivity and could absorb Cl^- more quickly, further enhancing the dissolution

Table 5
Fitted results of Nyquist plots for lined ductile iron pipes

Times	R_s (Ω cm^2)	R_f (Ω cm^2)	Q_f (μF cm^{-2})	n_f	R_{ct} (Ω cm^2)	Q_{dl} (μF cm^{-2})	n_{dl}
5 d	121.5	6,828	0.0023	1.000	33,283	528.70	0.511
10 d	127.3	5,541	0.0025	1.000	6,525	486.91	0.523
20 d	134.0	5,856	0.0024	0.999	7,473	352.90	0.626
30 d	159.1	5,940	0.0050	0.998	7,056	249.48	0.690
50 d	138.1	6,798	0.0052	0.993	8,018	505.73	0.545

Table 6
Fitted results of Nyquist plots for unlined ductile iron pipes

Times	R_s (Ω cm^2)	R_f (Ω cm^2)	Q_f (μF cm^{-2})	n_f	R_{ct} (Ω cm^2)	Q_{dl} (μF cm^{-2})	n_{dl}
5 d	20.13	338.9	0.0064	0.967	821.9	2,241.2	0.719
10 d	18.49	411.7	0.0066	0.980	615.4	3,718.7	0.505
20 d	18.50	369.6	0.0063	0.954	468.6	4,954.6	0.594
30 d	20.14	374.1	0.0067	0.952	425.5	5,574.3	0.557
50 d	23.02	337.0	0.00746	0.948	429.4	11,772	0.548

of iron [34]. Moreover, the obtained results of an associated double layer (Q_{dl}) varied from 2,241.2 to 11,772 μF cm^{-2}, higher than 1,000 μF cm^{-2}, further confirming the severe corrosion occurrence of ductile iron as a consequence of chloride and sulfate attack [33]. Therefore, the unlined ductile iron pipes were always in a state of severe corrosion during the 50 d experiments in water with high ionic strength.

3.5.3. Ductile iron pipes with 50% of cement mortar lining coverage

Fig. 9 shows the Nyquist plots of ductile iron pipes with 50% of cement mortar lining coverage. The ECM containing two-time constants in Fig. 9 was used to fit this impedance spectra. The fitted results are shown in Table 7.

The fitted R_{ct} all maintained at 514.7–824.7 Ω cm^2 throughout the experiments, lower than the values reported for the severe corrosion occurrence, illustrating the rapid corrosion reaction on the ductile iron surface [31]. The R_f and R_{ct} values decreased from the beginning of the experiments, showing the continuous corrosion reaction. This process might be attributed to localized corrosion existed in the incomplete interface between corrosion products and cement mortar lining coverage. The rough and inhomogeneous interface could not block the attack of chloride and sulfate on the inner iron surface and consequently induced the decreasing of R_{ct} values in the low frequency (10^{-2}–10^2 Hz) region. These results were consistent with the current understanding that corrosion reaction predominantly occurred at the imperfection's layers [17].

Additionally, the R_{ct} values in the case of ductile iron with 50% of lining were almost the same with that for unlined ductile iron, showing the poor protection ability to linings with significant defects. The fitted capacitance values showed a non-ideal behavior in the low-frequency region, with the n_{dl} variation from 0.123 to 0.438, revealing the existence of a heterogeneous lining/iron interface. The Q_{dl} values were much larger than 1,000 μF cm^{-2}, showing that the inner ductile iron was always in the severe corrosion period [33].

3.5.4. Ductile iron pipes with 90% of cement mortar lining coverage

Fig. 10 shows the Nyquist plots of ductile iron pipes with 90% of cement mortar lining coverage. The impedance spectra here showed a different phenomenon from the ductile iron with other proportions of cement mortar lining, illustrating the difference in the corrosion mechanisms.

The radius of impedance spectra in low-frequency region (10^{-2}–10^2 Hz) was minimal in the first 10 d, revealing the low corrosion resistance and rapid corrosion reaction on the ductile iron surface initially. It might be due to

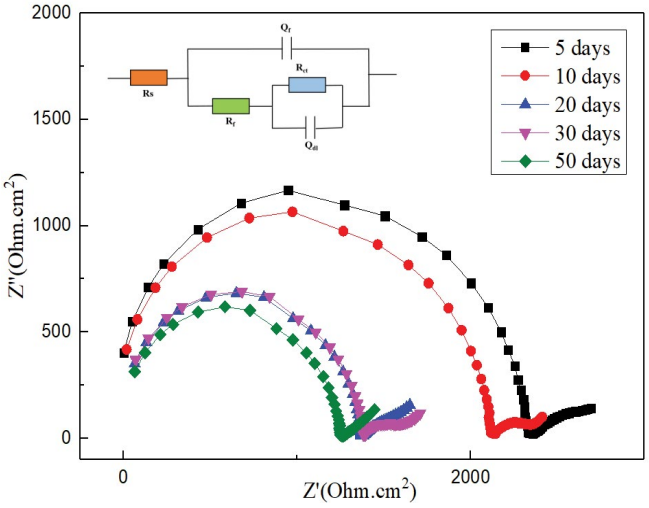

Fig. 9. Nyquist plots of ductile iron pipes with 50% of cement mortar lining coverage in water with high ionic strength.

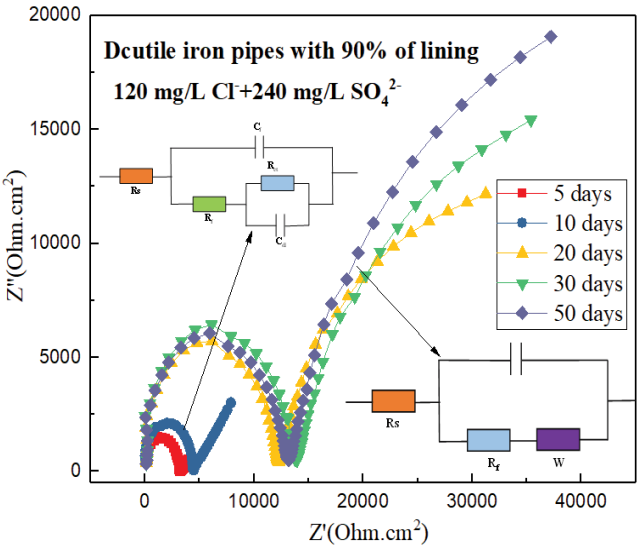

Fig. 10. Nyquist plots of ductile iron pipes with 90% of cement mortar lining coverage.

Table 7
Fitted results of Nyquist plots for ductile iron pipes with 50% of cement mortar lining coverage

Times	R_s (Ω cm^2)	R_f (Ω cm^2)	Q_f (μF cm^{-2})	n_f	R_{ct} (Ω cm^2)	Q_{dl} (μF cm^{-2})	n_{dl}
5 d	54.22	2,323	0.0023	0.996	757.9	4,468.5	0.438
10 d	42.00	2,005	0.0040	0.920	514.7	2,983.6	0.123
20 d	22.34	1,361	0.0033	0.868	620.8	6,401.1	0.356
30 d	21.80	1,345	0.0043	0.754	738.8	2,246.90	0.286
50 d	13.70	1,246	0.0039	0.623	824.7	11,392	0.360

the fact that chloride and sulfate anions could penetrate easily through the small hole and promoted the corrosion process efficiently.

After 10 d, the radius of impedance spectra in the high-frequency region and low-frequency region all increased with the exposure time. Moreover, the impedance spectra analyzed in the low-frequency region (10^{-2}–10^2 Hz) presented a large Warburg diffusion impedance, suggesting that the mass transfer process rather than the charge transfer resistance became the controlling factor for corrosion reaction. The preformed iron corrosion products might be combined with the hydrolysis products and hindered the dissolution of Fe^{2+} to some extent [10]. The presence of well-incorporated iron oxides and calcium hydrolysate, as shown in Fig. 6b also confirmed this phenomenon. The impedance spectra after 10 d were fitted with the ECM containing a Warburg diffusion resistance in Fig. 10. All the fitted results are shown in Table 8.

The fitted R_f and R_{ct} values were small in the first 10 d, demonstrating that the chloride and sulfate ions could penetrate through the small hole and accelerate the corrosion damage process for ductile iron. Subsequently, the fitted diffusion resistance tended to increase from 33,431 Ω cm^2 at 10 d to 51,171 Ω cm^2 at 50 d, indicating the increment of corrosion reaction resistance. It was speculated that the produced iron oxides might be deposited on the lining/iron interface, hence causing the increase of corrosion reaction resistance. Morris's research confirmed that the reinforcement would be passivated when the resistance was higher than 10,000 Ω cm^2 [35]. Thus, combing with SEM results, it can be concluded that the preformed iron corrosion products connected with the calcium hydrolysis products deposited on the iron/lining interface and passivated the iron surface after 10 d [36–38]. The associated Q_{dl} values also decreased from 245.3 mF cm^{-2} at 5 d to 132.53 mF cm^{-2} at 50 d, suggesting that the lining/iron double layer became denser. The associated diffusion coefficient (W_p) of the double-layer capacitance increased from 0.215 at 5 d to 0.848 at 50 d, indicating the increase of homogeneity of the lining/iron double layer.

3.6. Comparison of corrosion process for ductile iron pipes with different cement mortar lining coverage

The corrosion rates for ductile iron pipes with different cement mortar lining coverage placed in water with a high concentration of chloride and sulfate anions (120 mg L^{-1} Cl^- + 240 mg L^{-1} SO_4^{2-}) can be seen in Fig. 11.

The corrosion rate of lined ductile iron pipes was relatively lower initially (first 10 d), suggesting the protective effect of this lining on the inner iron surface, then followed by a gradual increase (after 10 d). It was speculated that the chloride and sulfate anions might react with the hydrolysis products of cement mortar lining ($Ca(OH)_2$) and form $CaCl_2$ or $CaSO_4$, thus causing the damage of cement mortar lining.

Compared with the corrosion rate of lined ductile iron, that of ductile iron with 90% of cement mortar lining showed a higher corrosion rate in the first 10 d, followed by a rapid decline in corrosion rate. The early rapid corrosion was thought to be caused by the quicker penetration of chloride and sulfate anions into the iron surface through the small blank holes initially (about 10% of the lining).

3.6.1. Interesting observation

The corrosion rate of the ductile iron pipes with 90% lining is higher than that of ductile iron with 50% lining or of bare iron. It was speculated that the ductile iron pipes with 90% ling (small hole) might be deemed as galvanic corrosion (a small anode and a large cathode) and resulted in more significant corrosion current density over a small anode area [39].

Consequently, more corrosion products were produced simultaneously for the ductile iron with 90% lining, thereby

Table 8
Fitted results of Nyquist plots for ductile iron pipes with 90% of cement mortar lining coverage

Times	R_s (Ω cm^2)	R_f (Ω cm^2)	Q_f (μF cm^{-2})	n_f	W_0 (Ω cm^{-2})	W_T (μF cm^{-2})	W_p
5 d	102.7	3,167	0.0020	1.000	3,792	21.61	0.215
10 d	114.1	4,495	0.0021	1.000	9,002	166.23	0.758
20 d	125.0	10,401	0.0019	1.000	33,431	140.24	0.823
30 d	147.1	10,922	0.0021	1.000	43,534	133.84	0.841
50 d	142.8	11,966	0.0019	1.000	51,171	132.53	0.848

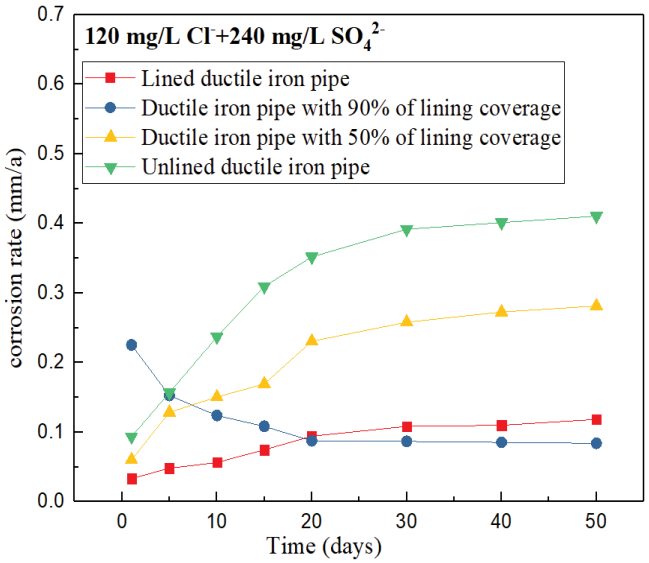

Fig. 11. Corrosion rate of ductile iron pipes with different cement mortar lining coverage placed in water with a high concentration of anions.

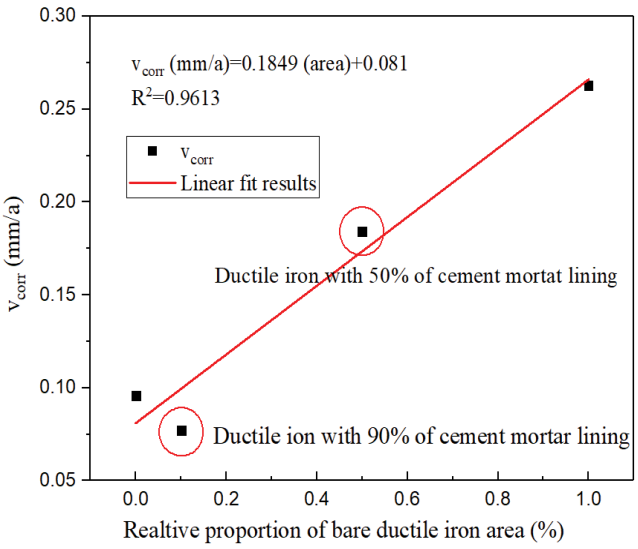

Fig. 12. Relationship between the corrosion rate and relative proportion of bare ductile iron area and the regression equation corresponding to the experimental data.

inducing a rapid decline in corrosion rate after 10 d. This decline could be possibly denoted to the superposition process involving the deposition of corrosion products and hydrolysis products of cement mortar lining. The corrosion rate of ductile iron with 90% lining was even lower than that of lined ductile iron, revealing that the interfacial zone rich in $CaCO_3$ and iron oxides could block the anions diffusion more effectively than the cement mortar lining itself.

During the enlargement of defects in cement mortar lining (the ratio of these defects was 50%), the corrosion situation changed significantly. The corrosion rate in this situation was always higher than that for ductile iron with 100% or 90% lining for the long term (after 10 d). In contrast to the ductile iron with small defects (90% lining), the corrosion products accumulation was not enough to cover the bare metal surface with significant defects, but caused the increment of surface roughness and promoted the corrosion process continuously. This result demonstrated that the chloride and sulfate anions could cause adverse corrosion damage for ductile iron pipe with significant lining defects, which is consistent with the current understanding that the corrosion process often occurred at the big breaks of the protective film or lining [17].

Additionally, unlined ductile iron showed a significantly higher corrosion rate than the other three. To be specific, the corrosion rate of unlined ductile iron was about 2–5 times higher than that with lined ductile iron pipes. Moreover, according to the level 3 standard of the uniform corrosion division [27], the corrosion of lined ductile iron in the first 10 d (<0.1 mm a^{-1}) was in the stage of almost unavailable corrosion (level 1). While the corrosion rate increased gradually due to the damage of chloride and sulfate, it came to the stage of available corrosion levels (level 2: 0.1–1.0 mm) after 10 d. Except for the lined ductile iron, the corrosion for ductile iron with 0%, 50% lining coverage all belonged to level 2, indicating the corrosion resistance evaluation as "available levels."

Interestingly, the corrosion rate of ductile iron with 90% lining became lower than that of lined ductile iron after 20 d. Thus, it can be believed that the well-incorporated iron oxides and calcium hydrolysate can hinder the anions diffusion more effectively than the cement mortar lining itself. Otherwise, the large defects (50% lining or unlined) could increase the corrosion risk of inner iron pipes under a high concentration of anions solution significantly.

The relationship between the average corrosion rate and the relative proportion of the bare ductile iron area can be seen in Fig. 12.

A roughly linear correlation between v_{corr} (mm a^{-1}) and relative proportion of bare ductile area with a slope of 0.1849 was fitted, implying a linearly increased promoting effect of iron area on the corrosion rate. The fitted results were much better for a uniform surface, which is the unlined and lined ductile iron. However, the deviation of v_{corr} and linear fitted results was significant for the ductile iron with 90% lining. According to the EIS results, the ductile iron with 90% lining was in the status of the small anode and large cathode that induced the galvanic corrosion and promoted the corrosion process [39]. However, the rapid corrosion process caused more corrosion products accumulation, which could be combined with the hydrolysis products of cement mortar lining and blocked the corrosion process. Thus, the inhomogeneous lining/iron interface composed of hydrolytic products and iron corrosion products might be responsible for this deviation [10].

4. Conclusions

The key finding of this study is that ionic strength could significantly affect the corrosion potential and corrosion current density by influencing the electron transfer resistance and mass transfer resistance, thereby influencing

the corrosion damage mechanisms. Results showed that the maximum corrosion potential of ductile iron pipes with different cement mortar lining coverage decreased as the increment of anions strength in a logarithm tendency, while the corrosion current density increases linearly with ionic strength. Moreover, the different cement lining coverage also affects the ductile iron corrosion process obviously. Results showed that (1) corrosion rate of unlined ductile iron was about 2–5 times higher than that of lined ductile iron, (2) the minor defects on the iron surface (90% of lining) experienced a severe corrosion period in the first 10 d; this process created a region rich in calcium oxides and iron oxides and limited the anions diffusion effectively afterward, (3) the cement mortar lining with large defects (50% of lining) showed poor protection ability on iron surface, (4) a rough linear correlation between average corrosion rate (mm a^{-1}) and relative proportion of bare ductile iron area was fitted.

The relatively higher ionic strength affected the corrosion process of ductile iron significantly in the present study, especially for the unlined iron pipes or lined iron pipes with large defects. While in the actual drinking water distribution systems, this erosion effect might be reduced due to the lower concentration of chloride and sulfate.

Acknowledgments

This study was supported by"Research on comprehensive integration of key technologies on water environment control and management in District of Beijing, Tianjin and Hebei province" (2018ZX07111006).

References

[1] AWWA, Cement-Mortar Lining for Ductile-Iron Pipe and Fittings for Water, American Water Works Association, 1996.
[2] L. Qiu, X. Zuo, Y. Tang, G. Yin, H. Tang, Electrochemical study on corrosion process of cement-mortar-lined ductile cast iron pipe under water supply, J. Nanjing Univ. Sci. Technol., 41 (2017) 217–225.
[3] H. Guo, Research on Electrochemical Corrosion Mechanisms of Water Supply Pipes, Tianjin University, Tianjin City, 2016.
[4] Y. Song, Y. Tian, X. Zhao, H. Guo, H. Zhang, Corrosion process of ductile iron with cement mortar linings as coatings in reclaimed water, Int. J. Electrochem. Sci., (2016) 7031–7047.
[5] J. Gong, M.L. Stephens, N.S. Arbon, A.C. Zecchin, M.F. Lambert, A.R. Simpson, On-site non-invasive condition assessment for cement mortar-lined metallic pipelines by time-domain fluid transient analysis, Struct. Health Monit., 14 (2015) 426–438.
[6] J. Sulikowski, J. Kozubal, The durability of a concrete sewer pipeline under deterioration by sulphate and chloride corrosion, Procedia Eng., 153 (2016) 698–705.
[7] M. Zhang, J. Chen, Y. Lv, D. Wang, J. Ye, Study on the expansion of concrete under attack of sulfate and sulfate–chloride ions, Constr. Build. Mater., 39 (2013) 26–32.
[8] R.B. Figueira, A. Sadovski, A.P. Melo, E.V. Pereira, Chloride threshold value to initiate reinforcement corrosion in simulated concrete pore solutions: the influence of surface finishing and pH, Constr. Build. Mater., 141 (2017) 183–200.
[9] U. Angst, B. Elsener, C.K. Larsen, Ø. Vennesland, Critical chloride content in reinforced concrete – a review, Cem. Concr. Res., 39 (2009) 1122–1138.
[10] S. Mundra, M. Criado, S.A. Bernal, J.L. Provis, Chloride-induced corrosion of steel rebars in simulated pore solutions of alkali-activated concretes, Cem. Concr. Res., 100 (2017) 385–397.
[11] S. Arzola-Peralta, J. Genescá Llongueras, M. Palomar-Pardavé, Study of the electrochemical behaviour of a carbon steel electrode in sodium sulfate aqueous solutions using electrochemical impedance spectroscopy, J. Solid State Electrochem., 7(2003) 283–288.
[12] L.J. Yang, Y.Z. Xu, Y.S. Zhu, L. Liu, X.N. Wang, Y. Huang, Evaluation of interaction effect of sulfate and chloride ions on reinforcements in simulated marine environment using electrochemical methods, Int. J. Electrochem. Sci., 11 (2016) 6943–6958.
[13] S.G. Dong, R.G. Du, Y.B. Gao, Y. Liang, Z.C. Guan, Effect of sulfate on corrosion behavior of reinforcing steel in simulated concrete pore solutions, ECS Trans.., 75 (2017) 17–23.
[14] O.S.B. Al-Amoudi, Attack on plain and blended cements exposed to aggressive sulfate environments, Cem. Concr. Compos., 24 (2002) 305–316.
[15] B. Pradhan, Corrosion behaviour of steel reinforcement in concrete exposed to composite chloride–sulfate environment, Constr. Build. Mater., 72 (2014) 398–410.
[16] F. Shaheen, B. Pradhan, Effect of chloride and conjoint chloride-sulfate ions on corrosion of reinforcing steel in electrolytic concrete powder solution (ECPS), Constr. Build. Mater., 101 (2015) 99–112.
[17] M. Zhao, M. Liu, G. Song, A. Atrens, Influence of pH and chloride ion concentration on the corrosion of Mg alloy ZE41, Corros. Sci., 50 (2008) 3168–3178.
[18] A.T. Horne, I.G. Richardson, R.M.D. Brydson, Quantitative analysis of the microstructure of interfaces in steel reinforced concrete, Cem. Concr. Res., 37 (2007) 1613–1623.
[19] J. Ming, J. Shi, W. Sun, Effect of mill scale on the long-term corrosion resistance of a low-alloy reinforcing steel in concrete subjected to chloride solution, Constr. Build. Mater., 163 (2018) 508–517.
[20] C. Alonso, C. Andrade, M. Castellote, P. Castro, Chloride threshold values to depassivate reinforcing bars embedded in a standardized OPC mortar, Cem. Concr. Res., 30 (2000) 1047–1055.
[21] J.O. Rivera-Corral, G. Fajardo, G. Arliguie, R. Orozco-Cruz, F. Deby, P. Valdez, Corrosion behavior of steel reinforcement bars embedded in concrete exposed to chlorides: effect of surface finish, Constr. Build. Mater., 147 (2017) 815–826.
[22] P. Refait, A.M. Grolleau, M. Jeannin, E. Francois, R. Sabot, Localized corrosion of carbon steel in marine media: galvaniccoupling and heterogeneity of the corrosion product layer, Corros. Sci., 111 (2016) 7031–7047.
[23] G. Liu, Y. Zhang, Z. Ni, R. Huang, Corrosion behavior of steel submitted to chloride and sulphate ions in simulated concrete pore solution, Constr. Build. Mater., 115 (2016) 1–5.
[24] X. Song, J. Wei, T. He, G. Li, Corrosion behavior of steel reinforcement embedded in cement mortar with surface treatment, J. Chin. Ceram. Soc., 37 (2009) 637–641.
[25] W.A. Badawy, R.M. El-Sherif, H. Shehata, Electrochemical behavior of aluminum bronze in sulfate-chloride media, J. Appl. Electrochem., 37 (2007) 1099–1106.
[26] Y.M. Kolotyrkin, Effects of anions on the dissolution kinetics of metals, J. Electrochem. Soc., 108 (1961) 209–216.
[27] Y. Lin, D. Yang, Corrosion and Corrosion Control Principle, China Petrochemical Press, Beijing, 2007.
[28] I. Oliveira, S.H.P. Cavalaro, A. Aguado, New kinetic model to quantify the internal sulfate attack in concrete, Cem. Concr. Res., 43 (2013) 95–104.
[29] Y. Yang, Y. Deng, Mechanical properties of hybrid short fibers reinforced oil well cement by polyester fiber and calcium carbonate whisker, Constr. Build. Mater., 182 (2018) 258–272.
[30] X. Shi, N. Xie, K. Fortune, J. Gong, Durability of steel reinforced concrete in chloride environments: an overview, Constr. Build. Mater., 30 (2012) 125–138.
[31] X. Zuo, K. Jiang, Y. Feng, Y. Tang, X. Sun, Analysis on depassivation process and chloride ion threshold of passive film on surface of ductile iron in simulated pore solution, J. Southeast Univ., 47 (2017) 392–396.
[32] H. Gerengi, Y. Kocak, A. Jazdzewska, M. Kurtay, H. Durgun, Electrochemical investigations on the corrosion behaviour of

reinforcing steel in diatomite- and zeolite-containing concrete exposed to sulphuric acid, Constr. Build. Mater., 49 (2013) 471–477.
[33] R. Vedalakshmi, N. Palaniswamy, Analysis of the electrochemical phenomenon at the rebar–concrete interface using the electrochemical impedance spectroscopic technique, Mag. Concr. Res., 62 (2010) 177–189.
[34] Y. Zou, J. Wang, Y.Y. Zheng, Electrochemical techniques for determining corrosion rate of rusted steel in seawater, Corros. Sci., 53 (2011) 208–216.
[35] W. Morris, A. Vico, M. Vazquez, Chloride induced corrosion of reinforcing steel evaluated by concrete resistivity measurements, Electrochim. Acta, 49 (2004) 4447–4453.
[36] M. Serdar, L.V. Žulj, D. Bjegović, Long-term corrosion behaviour of stainless reinforcing steel in mortar exposed to chloride environment, Corros. Sci., 69 (2013) 149–157.
[37] D.A. Koleva, J.H.W. de Wit, K. van Breugel, L.P. Veleva, E. van Westing, O. Copuroglu, A.L.A. Fraaij, Correlation of microstructure, electrical properties and electrochemical phenomena in reinforced mortar. Breakdown to multi-phase interface structures. Part II: Pore network, electrical properties and electrochemical response, Mater. Charact., 59 (2008) 801–815.
[38] M.O.G.P. Bragança, K.F. Portella, M.M. Bonato, C.E.B. Marino, Electrochemical impedance behavior of mortar subjected to a sulfate environment – a comparison with chloride exposure models, Constr. Build. Mater., 68 (2014) 650–658.
[39] M.K. Desantis, S. Triantafyllidou, M. Schock, D.A. Lytle, Mineralogical evidence of galvanic corrosion in drinking water lead pipe joints, Environ. Sci. Technol., 52 (2018) 3365–3374.